International Journal of Thermophysics, Vol. 25, No. 2, March 2004 (© 2004)

Impact of Thin Film Thermophysical Properties on Thermal Management of Wide Bandgap Solid-State Transistors[1]

A. N. Smith[2,3] and J. P. Calame[4]

Wide bandgap semiconductor solid-state transistors continue to have a wide array of applications that include power supplies, communications, electronic warfare, and multifunctional RF systems. Two viable wide bandgap semiconductor materials currently under investigation are silicon carbide (SiC) and gallium nitride (GaN). One interesting aspect of these devices is their ability to operate at elevated temperatures on the order of 500°C. At higher temperatures the heat capacity of semiconductors is constant, while the phonon mean free path is inversely proportional to the lattice temperature. This causes a significant reduction in the thermal conductivity over the operating temperature range. The submicron-scale conducting channels and junctions of wide bandgap devices can create highly localized heat fluxes on the order of several hundred kilowatts per square centimeter. Since these heat fluxes lead to localized hot spots within the electrically critical regions of the transistors, they can have a strong impact on device gain, power capability, and reliability. Quantifying the thermophysical properties of the underlying thin film materials is of critical importance for the accurate prediction of these localized temperature extremes.

KEY WORDS: gallium nitride; silicon carbide; thermal management; thin film thermal conductivity; wide bandgap.

[1] Paper presented at the Fifteenth Symposium on Thermophysical Properties, June 22–27, 2003, Boulder, Colorado, U.S.A.

[2] Mechanical Engineering Department, U.S. Naval Academy, Annapolis, Maryland 21402, U.S.A.

[3] To whom correspondence should be addressed. E-mail: ansmith@usna.edu

[4] Electronics Science and Technology Division, Naval Research Laboratory, Washington, D.C. 20375, U.S.A.

0195-928X/04/0300-0409/0 © 2004 Plenum Publishing Corporation

1. INTRODUCTION

Solid-state devices are widely used in microwave electronics applications. However, until recently these devices could not produce radio-frequency (RF) power levels high enough for many radar and communications transmitter applications. Although there are numerous commercial applications, the military is interested in developing multifunctional radar systems based on solid-state transistors and phased array technology [1, 2]. In addition to flexibility, solid-state systems would be lighter, require less volume, and could potentially be more affordable. Decreasing device size always comes at a cost, which is usually increased operating temperatures and power density levels. Figure 1 shows the projected thermal management requirements for microwave RF devices with large total gate widths. The heat flux values shown in Fig. 1 are based on a distributed heat load under the entire monolithic microwave integrated circuit (MMIC) die. The dies are typically several millimeters on each side and only several hundred microns thick. Since the heating occurs in the active region of the device, which is typically a much smaller area, the local heat flux values under the active region of the device are likely to be at least an order of magnitude higher.

A schematic of a typical MMIC power amplifier based on high electron mobility transistor (HEMT) technology is shown in Fig. 2. The

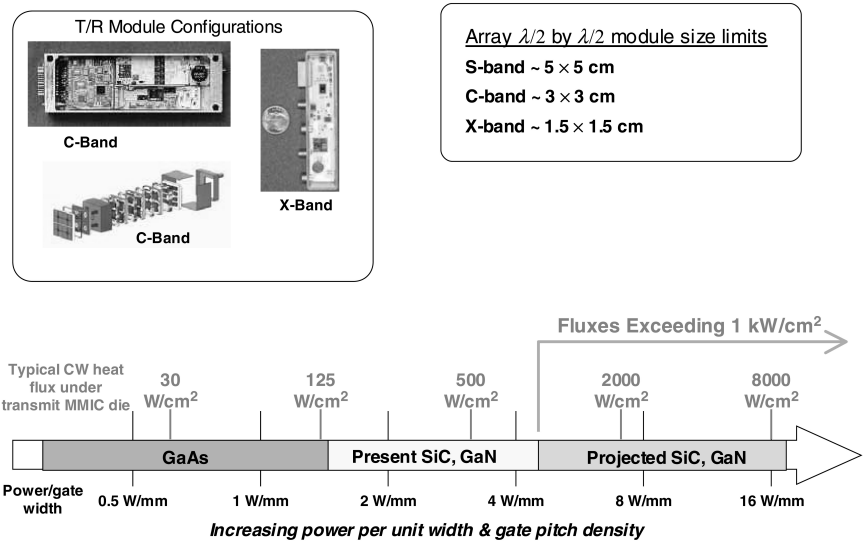

Fig. 1. Projected thermal management requirement for microwave RF amplifiers exceeding $1\ \mathrm{kW \cdot cm^{-2}}$.

dimensions that will be important to this study are the total gate width, the gate length L_G, and the gate-to-gate pitch spacing L_P. Two of the parameters typically reported for RF devices are the linear power density and the power added efficiency (PAE). The linear power density, P_{RF}, is the total RF output power divided by the total gate width. The PAE is the net increase in RF power divided by the total power applied to the device. These two values can be used to calculate the waste power, P_{waste}, dissipated as heat within the active area of the device. The assumption has been made in Eq. (1) that all losses occur in the active region of the transistor directly under the gate, and that the gain is sufficiently high (> 10 dB) so that the power from the RF input can be neglected.

$$\text{PAE} = \frac{P_{RF}}{P_{RF} + P_{waste}} \tag{1}$$

The heat is generated in the active region as shown in Fig. 2. The MMIC die is typically only several hundred microns thick. While this will provide some thermal spreading, the assumption of a uniform heat flux under the MMIC die is not reasonable.

Additional heat spreaders located under the MMIC die are required to distribute the heat flux to a more manageable level. The ultimate limit on the area over which the heat can be distributed is related to the RF wavelength. Phased array technology requires that the module spacing be no more than one half of the operating wavelength. Figure 3 shows a MMIC die mounted on a heat spreader and microchannel heat sink. Spreading the heat load alone is not sufficient, and the heat must ultimately be removed by an active heat sink. Figure 3 shows a microchannel cooling approach

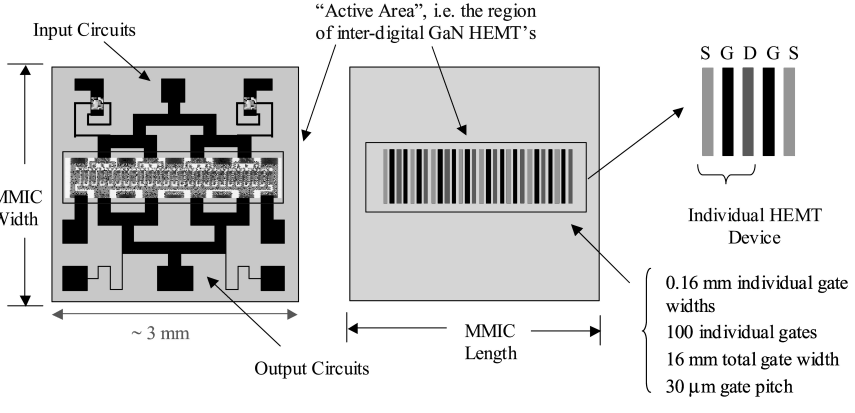

Fig. 2. Layout of the individual HEMT devices shown on the MMIC die.

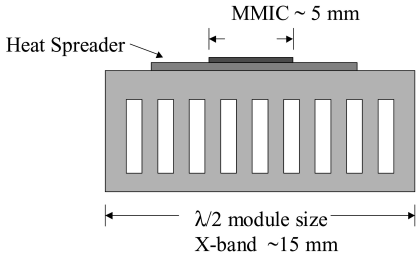

Fig. 3. Schematic based on general dimensions of a X-band MMIC die mounted on a microchannel based active cooling system.

that has been considered by several investigators [3, 4]. Another promising technique for the bulk removal of heat from these devices is spray cooling the bottom of the heat spreader [5].

The two materials that seem to be competing for this market are GaN and SiC. These materials are often described as wide bandgap semiconductors. Table I shows some of the relevant properties of both GaN and SiC including the bandgap, saturation velocity, electric field at saturation, and electron mobility. In general, wide bandgap semiconductors have lower dielectric constants, higher saturation velocities, and lower electron mobility than other semiconductors. However, the wider bandgaps allow these devices to operate at higher power levels since they can be biased with higher voltages.

The primary advantages of SiC are high thermal conductivity and the availability of single crystalline substrates. The electron mobility of SiC is adequate for operation at frequencies up to X-band (10 GHz) without any loss in performance. Very thin AlGaN layers have been deposited on GaN to form heterostructures, and the two-dimensional electron gases (2DEG) within these HEMT structures have exhibited electron mobilities on the order of 1500 $cm^2 \cdot V^{-1} \cdot s^{-1}$. This makes AlGaN/GaN devices suitable for

Table I. Material Properties of Competing Semiconductor Materials [1]

Material	Eg (eV)	μ ($cm^2 \cdot V^{-1} \cdot s^{-1}$)	v_s ($cm \cdot s^{-1}$)	E_s ($kV \cdot cm^{-1}$)
Si	1.12	1300	1×10^7	35
GaAs	1.43	5000	0.5×10^7	4
4H-SiC	3.2	500	2×10^7	100
GaN	3.4	1500	2.5×10^7	160

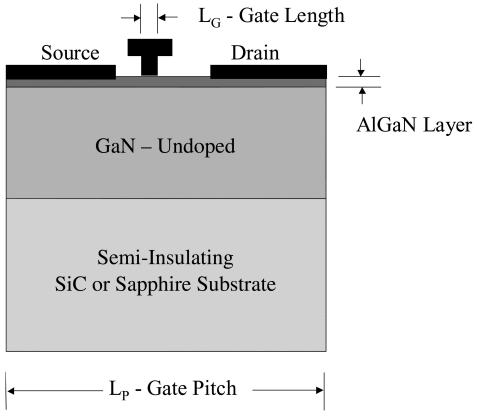

Fig. 4. Schematic of an individual AlGaN/GaN high electron mobility transistor.

operation up to 300 GHz [1]. The primary disadvantage of GaN is the lack of a bulk substrate material. The GaN films are typically grown on either sapphire or SiC substrates. The thermal conductivity of sapphire is about one tenth of SiC. It is important to keep in mind that sapphire substrates currently cost about twenty times less, so there are important tradeoffs between power capability and economic factors that depend on the particular systems application. Figure 4 shows a schematic of an AlGaN/GaN HEMT device. The thermal calculation preformed in this study will be based on this geometry. The AlGaN layer is typically on the order of 30 nm thick. Since this is much less than the 2 μm thick undoped GaN layer, the AlGaN layer will be neglected in these calculations.

2. TEMPERATURE DEPENDENCE OF THE THERMAL CONDUCTIVITY

Thermal conduction within a crystalline lattice is primarily due to acoustic phonons. Phonons are quantized lattice vibrations that represent the amplitude of vibration at a given frequency. They are generally treated as particles, which is analogous to assuming that the phonon is a localized wavepacket. According to kinetic theory, the thermal conductivity, λ, can be expressed by the following equation:

$$\lambda = \tfrac{1}{3} C v^2 \tau \tag{2}$$

where C is the specific heat, v is the velocity of the energy carrier, and τ is the mean free time between collisions. Acoustic phonons generally follow

a linear dispersion relation; therefore, the group velocity is assumed constant and equal to the speed of sound within the material. Thus, all the phonons are assumed to be traveling at a velocity equal to the speed of sound, which is independent of temperature. At very high temperatures all of the available energy states are excited and the phonon heat capacity is nearly constant. Therefore, the temperature dependence of the thermal conductivity is primarily related to the phonon collisional frequency.

In general, phonon-defect and phonon-phonon scattering processes dominate at room temperature and above. The phonon-defect collisional frequency, υ_{pd}, is independent of temperature, while the phonon-phonon collisional frequency, υ_{pp}, increases linearly with temperature [6]. Assuming that these scattering mechanisms are independent, the total collisional frequency is the sum of the different contributions. The mean free time between collisions is inversely proportional to the collisional frequency and can be expressed by the following equation:

$$\tau = \frac{1}{\upsilon_{pd} + \upsilon_{pp}} \tag{3}$$

Combining Eqs. (2) and (3) gives us a general form for the temperature dependence of the thermal conductivity [7]:

$$\lambda = \frac{1}{a + bT} \tag{4}$$

The coefficients a and b were determined by comparing this expression to literature values for the thermal conductivity of SiC [8], AlN [9], sapphire, and GaN. The results are given in Table II along with the density, specific heat, and the thermal conductivity at room temperature. These values were used in the thermal calculations presented in the next section. Figure 5 shows the thermal conductivity of SiC and sapphire plotted versus Eq. (3) for the values of a and b given in Table II.

Table II. Thermal Conductivity Temperature Dependent Coefficients and Other Thermophysical Properties for SiC, Sapphire, AlN, and GaN

$\lambda = 1/(a+bT)$	a ($K \cdot m \cdot W^{-1}$)	b ($m \cdot W^{-1}$)	λ ($W \cdot m^{-1} \cdot K^{-1}$) at 300 K	ρ ($kg \cdot m^3$)	Cp ($J \cdot kg^{-1} \cdot K^{-1}$)
4H SiC S.I.	-0.003	1.7×10^{-5}	475	3160	675
Sapphire	-0.022	16×10^{-5}	38	3980	764.5
AlN	-0.004	2.4×10^{-5}	319	3225	600
GaN[a]	-0.005	3.8×10^{-5}	156	2330	712

[a] Approximated using the room temperature values and Eq. (4).

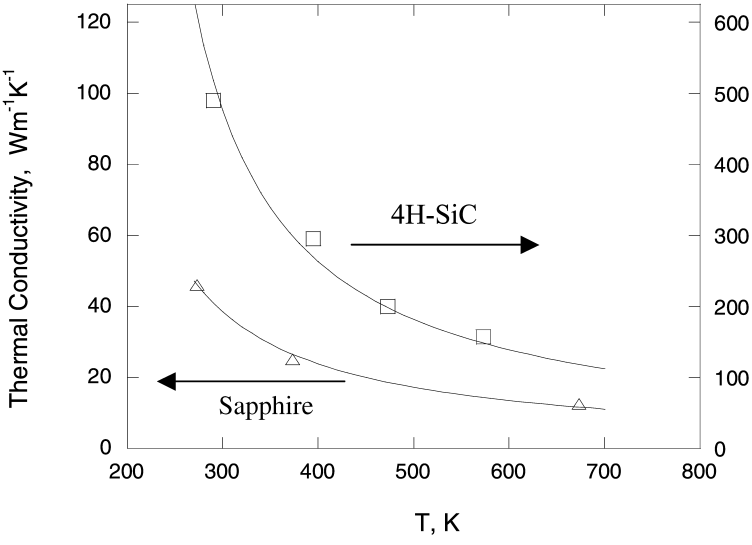

Fig. 5. Thermal conductivity of single crystalline sapphire substrate and high purity semi-insulating 4H SiC substrate (Muller et al. [8]).

The thermal conductivity of GaN was measured to be $\sim 130\ \mathrm{W \cdot m^{-1} \cdot K^{-1}}$ by Sichel and Pankove in 1997 [10]; their sample was a 400 μm thick GaN film grown by hydride vapor phase epitaxy (HVPE). This was significantly less than the upper limit of $170\ \mathrm{W \cdot m^{-1} \cdot K^{-1}}$ estimated by Slack [11] based on a scaling relationship using the Debye temperature. Asnin et al. [12] measured the thermal conductivity of GaN samples grown by metalorganic chemical-vapor deposition (MOCVD) and showed that the thermal conductivity of these samples was significantly higher than the HVPE films. These measurements were made using a scanning thermal microscopy (SThM) technique. Florescu et al. [13] used the same technique and reported values for the thermal conductivity as high at $200\ \mathrm{W \cdot m^{-1} \cdot K^{-1}}$ for completely coalesced films grown using a lateral epitaxial overgrowth (LEO) method.

Luo et al. [14] examined the temperature dependence of both LEO and HVPE films over the temperature range of 60 to 300 K. Their measurements were made using the 3ω technique. The LEO films consistently had higher values for the thermal conductivity, and the values reported at room temperature were around $155\ \mathrm{W \cdot m^{-1} \cdot K^{-1}}$. Luo et al. also showed that the temperature dependence of the GaN films was very similar to AlN. Figure 6 shows some of the values reported by Luo et al. along with

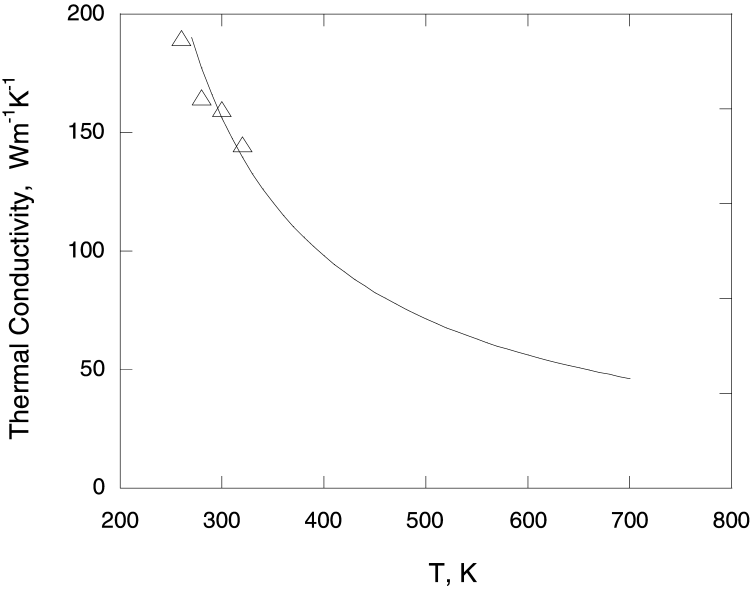

Fig. 6. Estimated temperature dependence of the thermal conductivity of GaN compared to low-temperature experimental results by Luo et al. [14].

a prediction over a higher temperature range using Eq. (4). The values for a and b were assumed to be similar to AlN and adjusted to agree with the room temperature values.

3. NUMERICAL SIMULATIONS

In order to quantify the impact of the thermophysical properties of GaN on the performance of high power devices, three cases will be examined: a sapphire substrate, a sapphire substrate that has been flip-chip bonded to AlN, and a SiC substrate. Recently, 22.6 W of CW power was produced with an AlGaN/GaN field effect transistor (FET) [15]. The $Al_{0.3}Ga_{0.7}N/GaN$ heterostructure was deposited on a 330 μm thick sapphire substrate. The thickness of the sapphire substrates represents a significant thermal resistance. Therefore, the substrate thickness was thinned to 50 μm by mechanical polishing. The total gate width was 16 mm, resulting in a linear RF power density of 1.41 $W \cdot mm^{-1}$. The PAE was reported at 41.9%, which means that the device is generating heat at a rate of 2 $W \cdot mm^{-1}$. The gate length for this device was given as 0.9 mm, and the distance between gates (the gate pitch) was given as 30 μm.

Using the above dimensions and Eq. (4) for the thermal conductivity, the computed temperature profile for the device is shown in Fig. 7. The computation was performed using the CFDRC-ACE+ simulation package. The assumption has been made in these calculations that the MMIC die is mounted on an active heat sink, and that this heat sink was capable of maintaining the lower boundary at 323 K. This is probably an optimistic assumption due to the high heat flux levels present on the back of the die, so the device was likely to be operating at a much higher temperature in the published experimental studies. The profile in Fig. 7 shows that for a heat load of $2\,W \cdot mm^{-1}$, there is a temperature difference of $\sim 150°C$ between the base of the substrate and the active region of the device.

It is apparent from Fig. 7 that the GaN layer is acting as a heat spreader moving the heat laterally away from the active region. The majority of the temperature drop ($\sim 120°C$) occurs over the sapphire substrate. Since the majority of the thermal resistance comes from the sapphire substrate, any uncertainty in the thermal conductivity of the thin film GaN layer would be less important.

The concept of flip-chip bonding GaN HEMT devices for the purpose of thermal management was first demonstrated by Thibeault et al. [16]. In essence the device is turned upside down and bonded to a higher thermal conductivity material such as aluminum nitride (AlN) which has a thermal

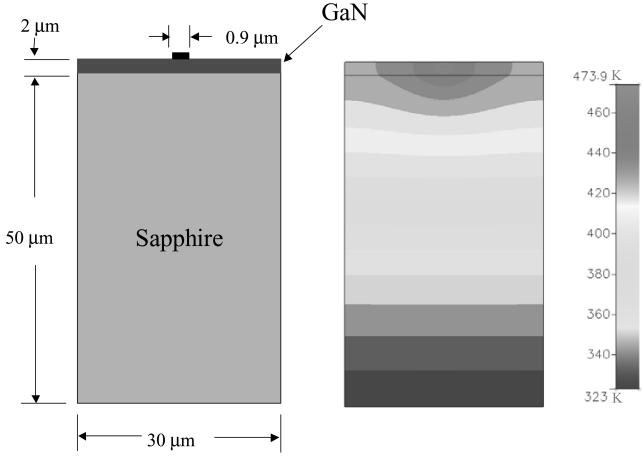

Fig. 7. Thermal model for GaN HEMT device on a thinned 50 μm sapphire substrate. An isothermal boundary condition of 323 K was assumed for the base of the substrate.

conductivity around 320 $W \cdot m^{-1} \cdot K^{-1}$ at room temperature compared to sapphire at $W \cdot m^{-1} \cdot K^{-1}$. The heat conduction path goes through the source and drain contacts. Thick Au pads are deposited onto the source and drain before that device is bonded to the AlN heat sink. Figure 8 shows the computed temperature profile for a GaN HEMT device that has been flip-chip bonded to an AlN heat sink. The dimensions used in this calculation were identical to those used in the previous example. The heat load was increased to 6.1 $W \cdot mm^{-1}$, which yielded a similar operating temperature of 200°C. Under these ideal conditions the flip-chip bonded device could handle an approximately 3 times greater head load. This is a very attractive option for the continued use of sapphire substrates and eliminates the need to thin the substrate material.

Once the device has been flipped and bonded, the heat must move laterally through the GaN layer before conducting through the Au contact pads to the AlN substrate. This increases the contribution to the overall thermal resistance from the GaN layer. In these calculations the contact resistance between the Au pads and the AlN substrate was neglected. Quantifying the thermal contact resistance of bonded interfaces will be a critical issue to the thermal management of these devices. This includes the bonded interface between the MMIC die and the heat spreader as shown in Fig. 3.

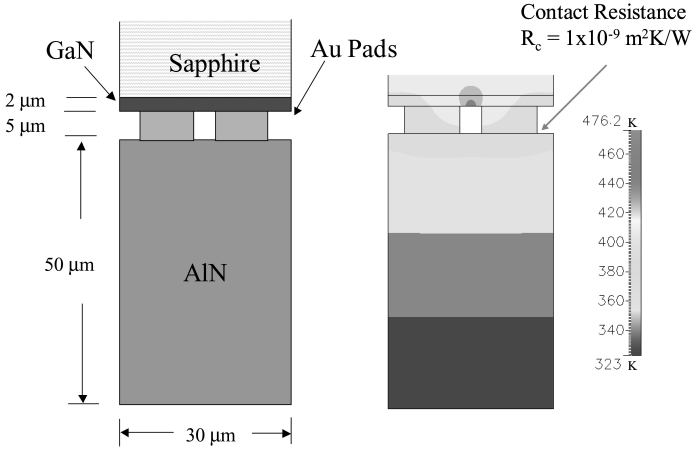

Fig. 8. Temperature profile for the device shown in Fig. 4 that has been flip chip bonded to an AlN Substrate. The Au pads were assumed to be 5 µm thick, and perfect thermal contact was assumed between the Au and the AlN.

The future of very high power MMIC dies certainly rest with SiC Substrates. The thermal conductivity of SiC is about ten times greater than sapphire. Since SiC is such a great thermal conductor, there is no need to consider flip-chip bonding. Figure 9 shows the temperature profile for the same device as shown in Fig. 7, except the substrate material has been replaced by SiC. The heat load could be increased to $10.2\,\mathrm{W \cdot mm^{-1}}$ while maintaining an operating temperature of 200°C. This is on the order of the waste power densities expected from GaN HEMT devices on SiC substrates. Again, SiC is such a good thermal conductor that most of the thermal resistance comes from the GaN layer. This effect is increased by the temperature-dependent properties, since the thermal conductivity of the GaN at 200°C is reduced to about one half of its value at room temperature. In this case it becomes critically important to understand the temperature-dependent, thin film properties of the GaN film. Figure 10 shows the heat flux for this device versus depth directly under the gate. The heat flux decays as a function of $1/r$ in the region near the gate, until the influence reaches the side boundaries. The heat flux then assumes a constant value of $\sim 33\,\mathrm{kW \cdot cm^{-2}}$. The peak heat flux of $\sim 1000\,\mathrm{kW \cdot cm^{-2}}$ occurs just under the gate.

In order to identify the impact of the thermal conductivity of the GaN film, the following study was performed. The operating temperature was

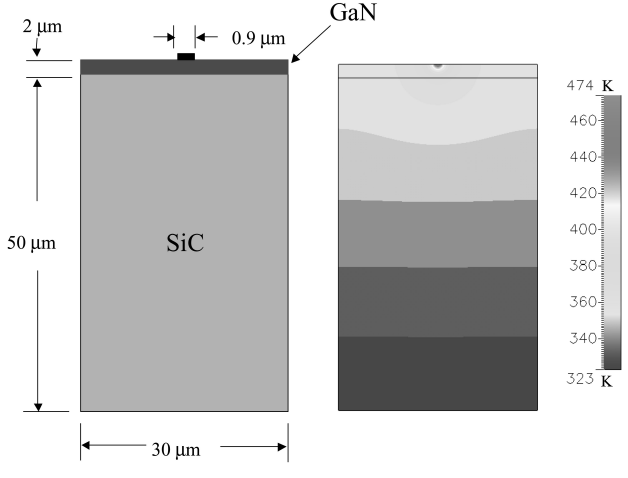

Fig. 9. Temperature profile for the device shown in Fig. 1 where the sapphire substrate has been replaced by a SiC substrate. The 50 μm thickness was retained for the purposes of comparison, although SiC substrates are typically ~ 150 to 300 μm thick.

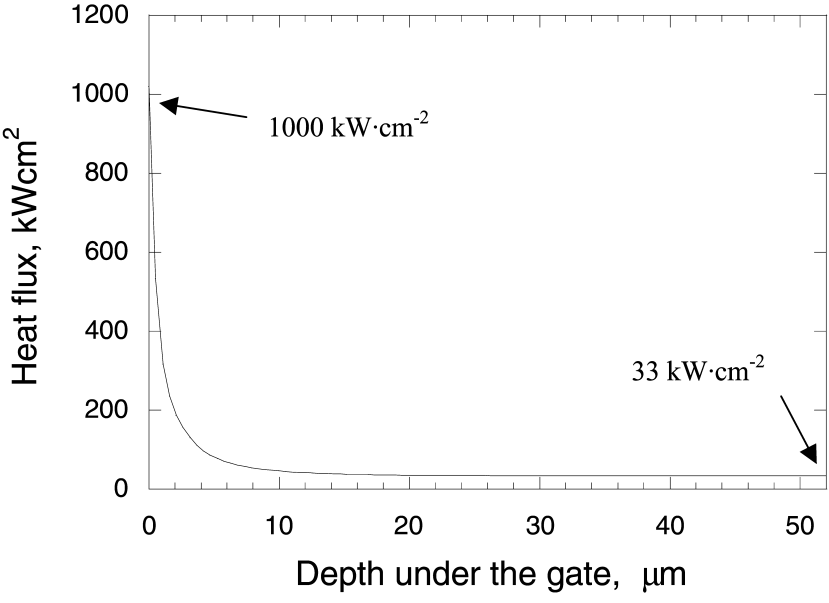

Fig. 10. Heat flux in the vertical direction for a AlGaN/GaN HEMT on SiC substrate shown as a function of depth directly underneath the center of the gate.

recalculated for each of the three cases previously described with different assumptions for the thermal conductivity. First, the calculations were performed assuming that the thermal conductivity of the GaN film was constant. The calculations were repeated assuming that the thermal conductivity was constant for the GaN film and the substrate materials. Since the thermal conductivity deceases with temperature, the operating temperature was lower in all cases. The results are shown in Table III. In the case of the sapphire substrate, changing the thermal conductivity of the sapphire had

Table III. Summary of the Operating Temperatures for the Three Cases Tested Using Temperature-Dependent Properties Versus Constant Values for the Thermal Conductivity

	P_{waste} ($W \cdot mm^{-1}$)	T_{max} (Table II: k-variable)	T_{max} (GaN: k-Constant)	T_{max} (All: k-Constant)
Sapphire	1.9	200°C	188°C	149°C
Flip-Chip AlN	6.1	200°C	165°C	152°C
SiC	10.2	200°C	162°C	150°C

the most significant effect. In the case of the SiC substrate, changing the thermal conductivity of the GaN film had the strongest influence. In all three cases assuming a constant value for the thermal conductivity seriously underpredicted the operating temperature of the device.

4. CONCLUSIONS

AlGaN/GaN devices deposited on SiC substrates are the most promising for high power RF devices. These devices combine the high electron mobility of the 2DEG AlGaN layer, with the thermal properties of a SiC substrate. It was shown that the temperature dependence of the thermal conductivity has a significant impact on the predicted operating temperature. Specifically, the thermal conductivity can be reduced by a factor of two at the typical operating temperature for these devices. Finally, it was shown that as advanced thermal management techniques are employed, quantifying the thermal properties of the GaN thin films becomes increasingly important. Flip-chip bonding creates a situation where the heat flow is forced to travel laterally through the GaN film, which increases its influence on the total thermal resistance. Similarly, using high thermal conductivity substrates reduces the overall thermal resistance to a point where the contribution from the GaN thin film becomes dominant.

ACKNOWLEDGMENTS

The authors are grateful for the financial support of the Office of Naval Research and for the advice and encouragement of Dr. Kristl Hathaway. One of the authors (A. N. Smith) would like to thank the Naval Academy Research Council for their financial support.

REFERENCES

1. R. J. Trew, *Proc. IEEE* **90**:6 (2002).
2. R. C. Clarke and J. W. Palmour, *Proc. IEEE* **90**:6 (2002).
3. D. B. Tuckerman and R. F. Pease, *IEEE Electron Device Letters* **2**:5 (1981).
4. J. P. Calame, F. Wood, and R. Myers, *GOMACTech Conference* (2003).
5. B. A. Kopp, A. J. Billups, and M. H. Luesse, *Microwave Journal* **44**:12 (2001).
6. J. M. Ziman, *Electrons and Phonons* (Oxford University Press, London, 1960).
7. T. Li, P. P. Ruden, J. D. Albrecht, M. G. Ancona, and R. Anholt, *Wide-Bandgap Electronic Devices* **622** (2000).
8. S. G. Muller, M. F. Brady, W. H. Brixius, G. Fechko, R. C. Glass, D. Henshall, H. M. Hobgood, J. R. Kenny, R. Leonard, D. Malta, A. Powell, V. F. Tsvetkov, S. Allen, J. Palmour, and C. H. Carter, *Materials Science Forum* **389–393** (2002).
9. G. A. Slack, R. A. Tanzilli, and R. O. Pohl, *J. Phys. Chem. Solids* **48**:7 (1987).

10. E. K. Sichel and J. I. Pankove, *J. Phys. Chem. Solids* **38** (1977).
11. G. A. Slack, *J. Phys. Chem. Solids* **34** (1973).
12. V. A. Asnin, F. H. Pollack, J. Ramer, M. Schurman, and I. Ferguson, *Appl. Phys. Lett.* **75**:9 (1999).
13. D. I. Florescu, V. M. Asnin, F. H. Pollak, A. M. Jones, J. C. Ramer, M. J. Schurman, and I. Ferguson, *Appl. Phys. Lett.* **77**:10 (2000).
14. C. Luo, D. R. Clarke, and J. R. Dryden, *J. Electonic Materials* **30**:3 (2001).
15. Y. Ando, Y. Okamoto, H. Miyamoto, N. Hayama, T. Nakayama, K. Kasahara, and M. Kuzuhara, *Int. Electron Devices Meeting*, Cat. No. #01CH37224 (2001).
16. B. J. Thibeault, B. P. Keller, Y. F. Wu, P. Fini, U. K. Mishra, C. Nguyen, N. X. Nguyen, and M. Le, *Int. Electron Devices Meeting*, Cat. No. #97CH36103 (1997).